Stability and DNA Binding Ability of the DNA Binding Domains of Interferon Regulatory Factors 1 and 3†

Victoria V. Hargreaves, Elena N. Makeyeva, Anatoly I. Dragan, and Peter L. Privalov*

Department of Biology, Johns Hopkins University, Baltimore, Maryland 21218

Received June 10, 2005; Revised Manuscript Received August 10, 2005

ABSTRACT: The thermodynamic properties and DNA binding ability of the N-terminal DNA binding domains of interferon regulatory factors IRF-1 (DBD1) and IRF-3 (DBD3) were studied using microcalorimetric and optical methods. DBD3 is significantly more stable than DBD1: at 20 °C the Gibbs energy of unfolding of DBD3 is −28.6 kJ/mol, which is 2 times larger than that of DBD1, −14.9 kJ/mol. Fluorescence anisotropy titration experiments showed that at this temperature the association constants with the PRDI binding site are 1.1×10^6 M^{-1} for DBD1 and 3.6×10^6 M^{-1} for DBD3, corresponding to Gibbs energies of association of −34 and −37 kJ/mol, respectively. However, the larger binding energy of DBD3 is due to its larger electrostatic component, while its nonelectrostatic component is smaller than that of DBD1. Therefore, DBD1 appears to have more sequence specificity than DBD3. Binding of DBD1 to target DNA is characterized by a substantially larger negative enthalpy than binding of DBD3, implying that the more flexible structure of DBD1 forms tighter contacts with DNA than the more rigid structure of DBD3. Thus, the strength of the DBDs' specific association with DNA is inversely related to the stability of the free DBDs.

Prompt and regulated cellular response is central to host defense against bacterial and viral pathogens. It is coordinated by a genetic network controlled by various transcription factors, particularly the interferon regulatory factors, IRFs. All IRFs have two domains: the N-terminal DNA binding domain (DBD), which is homologous among the family members, and a C-terminal transactivation domain (*1*). The crystal structures of the DBDs of IRF-1−IRF-4 have been determined in complex with consensus DNA and exhibit a high degree of similarity (*2*−*5*). They bind the major groove of DNA at the consensus site 5′-AANNGAAA-3′ and cause the DNA to bend toward the protein by approximately 20° (Figure 1). Topologically, these domains share the winged helix−turn−helix (wHTH) motif; however, they bear no sequence homology with other DNA-binding proteins in this category, and a cluster of five tryptophans and two extended loops makes these DBDs unique.

Notwithstanding a topological similarity of all IRF DBDs, a detailed comparison of the existing structures, particularly the DBDs of IRF-1 and IRF-3, which will be denoted here just as DBD1[1] and DBD3, respectively, reveals certain differences. It appears that DBD3 has more β-conformation, which forms a more extensive sheet contacting the α1 helix, and the content of the α-helical conformation in this DBD is somewhat higher. Also, the interactions with DNA loops L1 and L3 differ considerably in their extent. The structures of the DBDs of IRF-1 and IRF-3 in the absence of DNA are unknown, but the solution structure of free IRF-2 DBD has been determined and shows that the loops are highly disordered and undergo large structural changes upon binding DNA (*6*, *7*).

In this paper, we report the energetic bases of the structure of the DBDs of IRF-1 (DBD1) and IRF-3 (DBD3) and their complexes with the consensus DNA.

MATERIALS AND METHODS

Proteins and DNA Duplexes. Separate plasmids encoding the 113 N-terminal amino acids of DBD1 and DBD3 were kindly provided by C. Escalante. Both proteins were expressed in BL21(DE3)pLysS cells. The expression and purification of DBD1 have been described previously (*8*). DBD3 was expressed, and cell pellets were collected and lysed by sonication. DBD3 was separated by ammonium sulfate fractionation, pelleting at 70% saturation, and dialyzed against buffer A (200 mM sodium phosphate, 0.5 M NaCl, and 50 mM imidazole). His-tagged DBD3 was passed over an FPLC nickel-charged HiTrap chelating column (Amersham Biosciences) and eluted with a 50 to 500 mM imidazole gradient in buffer A. The His tag was removed by overnight digestion with thrombin, and the protein was separated from free tag by another round of Hi Trap chelating column chromatography. DBD3 was concentrated and dialyzed

† This work was supported by NIH Grant GM48036-12.

* To whom correspondence should be addressed. Telephone: (410) 516-6532. Fax: (410) 261-1064. E-mail: privalov@jhu.edu.

[1] Abbreviations: DBD1, IRF-1 DNA binding domain; DBD3, IRF-3 DNA binding domain; PRDI and PRDIII, positive regulatory domain I and III DNA binding sites, respectively; TCEP, reducing agent tris-(2-carboxyethyl)phosphine HCl; FAM, 5,6-carboxyfluorescein; T_t, equilibrium transition temperature at which half of the molecules are in the unfolded state in the equilibrium process; C_p, partial molar heat capacity; ΔC_p, heat capacity increment upon unfolding of the protein; m_{unf}, parameter that shows the increase of the denaturant accessible protein surface upon unfolding; ΔH_{unf} and ΔG_{unf}, enthalpy and Gibbs energy of protein unfolding, respectively; ΔH^a, ΔS^a, and ΔG^a, enthalpy, entropy, and Gibbs energy of association, respectively.

10.1021/bi051115o CCC: $30.25
Published on Web 10/05/2005

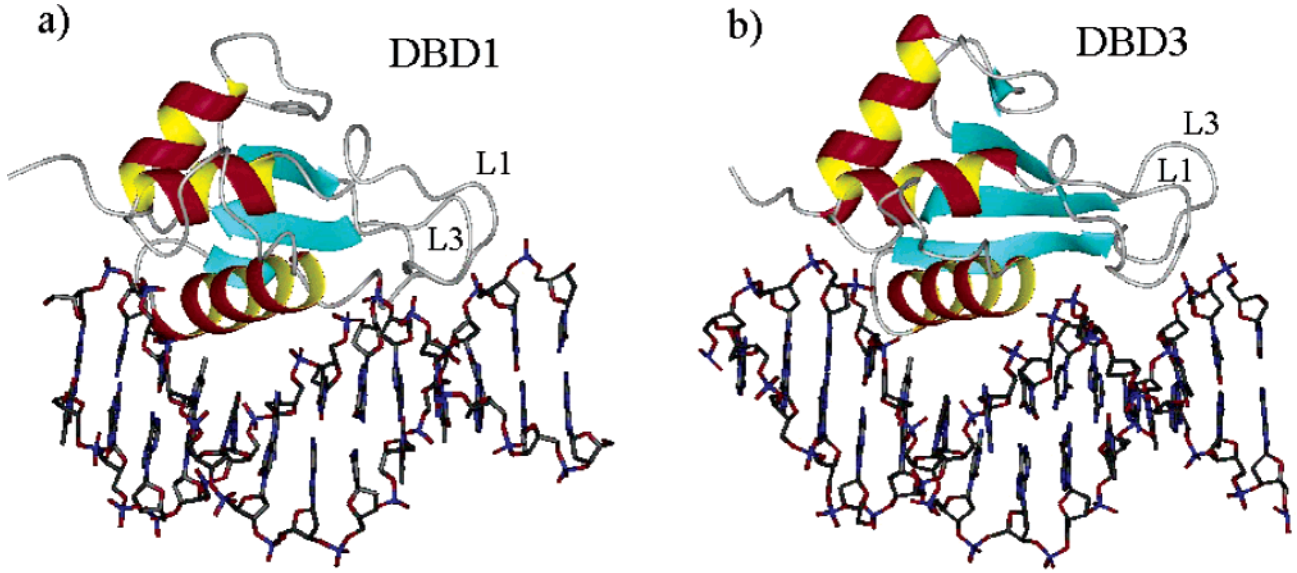

FIGURE 1: Crystal structures of the DBD1 (a) and DBD3 (b) complexes with the consensus PRDI and PRDIII DNAs, respectively (*2*, *4*).

against the appropriate buffer. Concentrations of DBD1 were determined using an extinction coefficient (ϵ_{280}) of 36 820 M^{-1} cm^{-1}. Concentrations of DBD3 were determined using an extinction coefficient (ϵ_{280}) of 31 010 M^{-1} cm^{-1}. The purity of all proteins used was checked by chromatography and mass spectrometry and found to be better than 98%. All studies of DBD1 containing cysteine were carried out in the presence of 1 mM TCEP as a reducing agent.

DNA containing the positive regulatory domain I (PRDI) site from the human interferon-β enhancer was used as a target for the IRF DBDs in calorimetric and optical experiments. For studying the thermodynamics of association between the proteins and DNA by calorimetry, a 13 bp duplex containing the PRDI site was used (a). For fluorescence anisotropy experiments, a 13 bp DNA duplex containing the PRDI site (b) and a 17 bp noncognate DNA duplex (c) were used, each labeled at one 5′ end with FAM:

(a) 5'-GAG**AAGTGAAA**GT-3'
3'-CTC**TTCACTTT**CA-5'
(b) 5'-GAG**AAGTGAAA**GT-3'
3'-CTC**TTCACTTT**CA-5'-FAM
(c) FAM-5'-ACTATAACAATACAAG-3'
3'-TGATATTGTTATGTTC-5'

All oligonucleotides were purchased from Integrated DNA Technologies, Inc. The oligonucleotides were purified by anion exchange FPLC on a Mono-Q column, using a linear 0.1 to 1.0 M NaCl gradient in 10 mM Tris-HCl buffer (pH 7.0), 1 mM EDTA, and 20% acetonitrile. The DNA was precipitated with ethanol, pelleted, and then air-dried.

Concentrations of single strands and duplexes were determined from the A_{260} of the nucleotides after complete digestion by phosphodiesterase I (Sigma) in 100 mM Tris-HCl (pH 8.0). To determine the concentration of labeled single strands, the additional contribution of FAM absorption at 260 nm (E_{260} = 28 000 M^{-1} cm^{-1}) was taken into account.

DNA duplexes were prepared by mixing the complementary oligonucleotides in equimolar amounts, heating to 70 °C, and cooling slowly to room temperature. Solutions of duplex DNA for the experiments were prepared by extensive dialysis against the desired buffer.

Spectropolarimetry. CD measurements were carried out using a Jasco-710 spectropolarimeter equipped with a Peltier PTC-3481 temperature controller. Measurements of the ellipticity of the samples were obtained in various buffers using a 1 mm Suprasil quartz cell. Spectra were monitored over the wavelength range of 190−270 nm.

Differential Scanning Calorimetry. DSC was performed on a Nano-DSC calorimeter from Calorimetry Sciences Corp. (Lindon, UT) with a cell volume of 0.328 mL. Details of the performance of this instrument and the experimental procedures are given elsewhere (*10*, *11*). Solutions for the calorimetric experiments were extensively dialyzed against solvent for at least 12 h at 4 °C. Results were analyzed using the C_p CALC program supplied with the Nano-DSC (*12*).

GdmCl Denaturation. Fitting and ΔG determination of unfolding by GdmCl, monitored by the change in the intrinsic fluorescence and ellipticity at 215 nm, were as described previously (*15*).

Fluorescence Anisotropy Measurements. Fluorescence anisotropy, corrected for the *G*-factor, was measured on a SPEX FluoroMax-3 spectrofluorimeter under control of DataMax software (version 2.10). Excitation and registration of emission were at 490 and 520 nm, respectively. The instrument has a thermostated cell holder and software-controlled water bath. A 0.4 cm path length quartz Suprasil cell was used. All measurements were conducted in 10 mM sodium phosphate buffer (pH 7.4). Association constants of the DBDs with the PRDI−DNA duplex labeled with a fluorophore were evaluated by direct fitting of the measured binding isotherms as described previously (*9*). The fitting procedure assumed a 1:1 equilibrium between DBD and DNA. The association constants were measured at three fixed temperatures, 10, 20, and 30 °C, and provided the Gibbs energies of association at these temperatures.

Isothermal Titration Calorimetry. ITC was performed on a Nano-ITC Series III instrument from Calorimetry Sciences Corp. with a cell volume of 1.25 mL. Concentrated protein solutions (700 μM) were placed in the syringe and DNA (50 μM) in the cell. The protein solution was titrated in 5 μL increments at 200 s intervals into the DNA solution

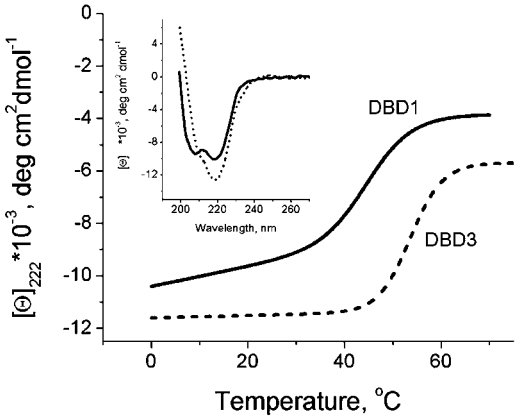

FIGURE 2: CD spectra of DBD1 (—) and DBD3 (- - -) at 0 °C in solutions at pH 6.0 and 100 mM NaCl (inset) and the change in mean residue ellipticity at 222 nm upon heating.

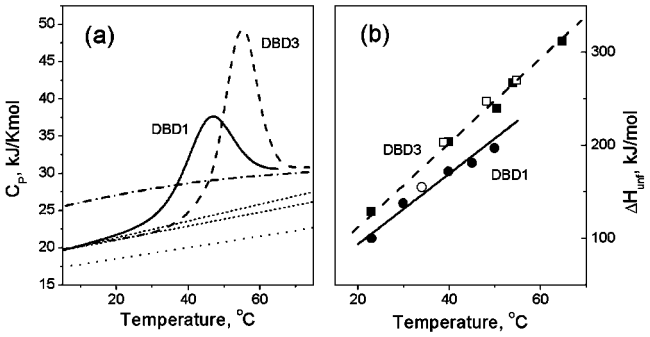

FIGURE 3: (a) Partial heat capacity of DBD1 (—) and DBD3 (— — —) in solutions at pH 7.4. The dotted line shows the heat capacity function expected for BPTI, a protein with a rigid stable structure. The dashed and dotted line shows the heat capacity function expected for the fully unfolded DBDs. (b) Dependence of the unfolding enthalpies of DBD1 (—) and DBD3 (— — —) on the temperature of unfolding determined by DSC (open symbols) and CD (closed symbols) in solutions with different pHs.

thermostated at the desired temperature. Samples of DNA and protein were prepared with the same batch of buffer to minimize artifacts due to minor differences in buffer composition. In separate experiments, the heats of dilution of the DNA into the solvent were measured and corresponding corrections were made. The results of the titration experiments were analyzed using the Bindwork program, which is included with the ITC instrument from CSC. Calorimetric measurements were carried out in the range of 5−30 °C with a 5 °C interval.

RESULTS

Stability of the DBDs. According to the circular dichroism (CD) spectra of free DBD1 and DBD3 (Figure 2), they differ significantly in their content of regular conformations: at 0 °C DBD1 has ~3% less α and β conformations than DBD3. The content of these regular conformations in DBD1 decreases faster upon heating than that of DBD3, and it unfolds cooperatively at significantly lower temperatures than DBD3. The van't Hoff enthalpy (ΔH^{vH}) calculated from the sharpness of the transition for DBD1 is 181 ± 5 kJ/mol at the transition temperature (45.4 °C); for DBD3, the van't Hoff enthalpy H_{unf}^{vH} is 267 ± 5 kJ/mol at the transition temperature (53.7 °C).

These CD results were confirmed by differential scanning calorimetry (Figure 3a). It is also seen that the cooperative unfolding of DBD3 takes place at significantly higher temperatures and proceeds with a much more pronounced and sharp heat absorption peak than the unfolding of DBD1, the excess heat absorption of which is more diffuse. The dashed line in this figure shows the heat capacity expected for the fully unfolded polypeptide chains of these proteins calculated by summing the partial specific heat capacities of the constituent amino acid residues (*13*, *14*). The correspondence of the calculated heat capacity function of the unfolded polypeptide chain to the calorimetrically measured heat capacity of the heat-denatured DBDs illustrates that thermal denaturation leads to the complete unfolding of these proteins. The dotted line shows the heat capacity function for a fully folded protein of comparable size such as bovine pancreatic trypsin inhibitor (BPTI).

It is notable that at 5 °C the partial heat capacity of DBD1 is almost similar to that of DBD3 and both are significantly larger than what is expected for BPTI, a protein with a compact, rigid structure. With the temperature increase, the heat capacity of DBD1 increases faster than that of DBD3. The larger heat capacity slope of DBD1 implies that the thermal motions of this protein are more intense than those of DBD3. Thus, the structure of DBD1 appears to be more flexible and loose. It should be noted that the tendency of DBD1 to aggregate and form disulfide cross-links upon unfolding prevented accurate calorimetric measurement of the enthalpy of its unfolding. Therefore, most of the data for this protein were obtained by the van't Hoff analysis of the CD melting profiles since that requires much lower concentrations of protein than calorimetric experiments.

As the pH decreases, the stability of the DBDs drops and, correspondingly, their enthalpies of unfolding decrease. The enthalpies of unfolding of DBD1 and DBD3 in solutions with different pHs are plotted against the transition temperatures, T_t, in Figure 3b. The calorimetric and van't Hoff enthalpies are in good correspondence for both DBDs, showing that their temperature-induced unfolding represents a highly cooperative process that can be modeled by a two-state transition. The slope of the enthalpy function corresponds to the heat capacity effect of protein unfolding ($\partial\Delta H/\partial T = \Delta C_p$). The heat capacity effect of unfolding is 3.8 ± 0.1 kJ K^{-1} mol^{-1} for DBD1 and 4.5 ± 0.1 kJ K^{-1} mol^{-1} for DBD3, in good correspondence with the direct observation of the heat capacity increment upon unfolding (Figure 3a). The fact that unfolding of DBD3 results in a larger heat capacity increment indicates that this protein has a more extensive hydrophobic core.

Using the determined transition temperature, the transition enthalpy, and the heat capacity effect of unfolding, and assuming that this effect does not change considerably with temperature, one can determine the Gibbs energy of protein stabilization at any temperature according to the following equation:

$$\Delta G(T) = \Delta H_t(1 - T/T_t) - \Delta C_p[(T_t - T) - T\ln(T_t/T)] \quad (1)$$

For 20 °C, the Gibbs energy of stabilization of DBD1 is −14.0 ± 1.0 kJ/mol and that of DBD3 is −27.7 ± 1.0 kJ/mol; i.e., DBD3 is approximately 2 times more stable than DBD1. Using the enthalpies of unfolding at 20 °C, which

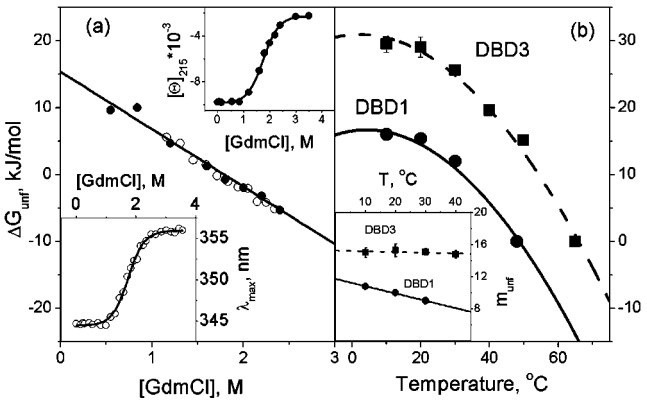

FIGURE 4: (a) GdmCl-induced unfolding of DBD1 at 20 °C followed by the change in the wavelength of maximal fluorescence emission (○) and ellipticity at 215 nm (●) (insets). Both methods give very similar ΔG_{unf} values, and their dependence on the GdmCl concentration is approximated by the linear function. (b) Gibbs energies of unfolding of DBD1 (—) and DBD3 (− − −) at different temperatures determined by extrapolation to zero denaturant concentration. The m_{unf} values of DBD1 (—) and DBD3 (- - -) vs temperature derived from the GdmCl unfolding experiment (inset).

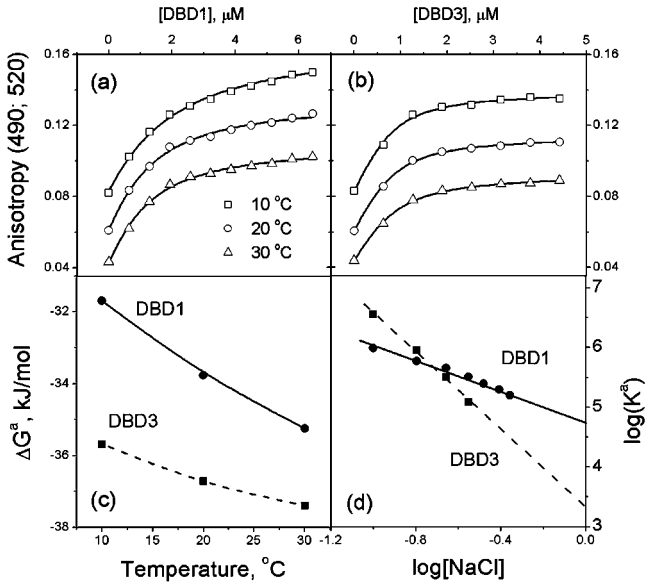

FIGURE 5: Isotherms of DNA binding by DBD1 (a) and DBD3 (b) determined at various fixed temperatures. (c) The Gibbs energies of association of DBD1 (—) and DBD3 (- - -) with the target DNA duplex plotted against the temperature of the titration experiment. (d) Dependencies of log(K^a) on log[NaCl] for association of DBD1 (—) and DBD3 (- - -) with the target DNA.

are 99 ± 5 and 130 ± 5 kJ/mol for DBD1 and DBD3, respectively (Figure 3b), one can determine the entropy factors of unfolding of these DBDs ($T\Delta S = \Delta H - \Delta G$). These are 85 ± 6 and 102 ± 6 kJ K^{-1} mol^{-1} for DBD1 and DBD3, respectively.

The large difference in the stabilities of these two DBDs according to analysis of their temperature-induced unfolding was confirmed by studying their unfolding by guanidine hydrochloride (GdmCl). Chemical denaturation is advantageous because it did not cause the DBDs to aggregate, even at neutral pHs. Unfolding by GdmCl was monitored by the change in intrinsic fluorescence and ellipticity at 215 nm (insets in Figure 4a). The results obtained by these parameters were practically identical, demonstrating that unfolding by GdmCl is a highly cooperative process, which can be described by a two-state transition. The Gibbs energies calculated on the basis of this model exhibit a linear dependence on the GdmCl concentration (Figure 4a). Extrapolation of this functional dependence to zero denaturant concentration gives the Gibbs energy of stabilization of the protein's native structure at the temperature of this experiment (*15*). The plots of these values versus temperature for DBD1 and DBD3 are presented in Figure 4b. At 20 °C, the Gibbs energy of unfolding of DBD1 is −15.4 ± 1.0 kJ/mol and that of DBD3 is −28.6 ± 1.0 kJ/mol. These values are very close to those determined by the temperature-induced unfolding of the DBDs. Thus, both methods demonstrate that the structure of DBD3 is significantly more stable than the structure of DBD1.

Another important parameter provided by the denaturant-induced unfolding is the slope of the ΔG_{unf} dependence on the concentration of the denaturant (m_{unf}), the parameter that shows the increase of the denaturant accessible protein surface upon unfolding (*15*). As shown in the inset of Figure 4b, m_{unf} is significantly smaller for DBD1, and its dependence on temperature decreases more quickly. Since the denaturant-exposed surfaces of these two DBDs in the unfolded state are very similar because their sequences are similar, one can conclude that in the native state, DBD1 has more extended surface exposed to denaturant. That is, the structure of DBD1 is looser than the structure of DBD3, and the looseness of DBD1 increases as the temperature increases. This conclusion is in accord with the results of the heat denaturation experiments.

Association of the DBDs with DNA. Detailed thermodynamic description of a protein−DNA complex entails specification of the following information: the equilibrium constant; the Gibbs energy, which is derived from the association constant [$\Delta G^a = -RT \ln(K^a)$]; the enthalpy of association (ΔH^a); and the entropy of association (ΔS^a), which is determined using the enthalpy and Gibbs energy of association [$\Delta S^a = (\Delta H^a - \Delta G^a)/T$]. It is particularly important that these parameters be determined at various temperatures and salt concentrations. The dependence of the association enthalpy on temperature provides the heat capacity effect of binding ($\partial \Delta H^a / \partial T = \Delta C_p{}^a$), which is important for estimating the role of the hydration effect, i.e., the change in water accessible surfaces (*16*−*18*). The dependence of the equilibrium constant on ionic strength provides the electrostatic component of the binding energy. The association enthalpy can be measured only by an isothermal titration calorimeter (ITC), while the association constant can be determined by any instrument that is sensitive to binding. In our experience, the most efficient method of studying protein−DNA association is fluorescence anisotropy titration, which works over a broad range of reactant concentrations (*19*).

The binding isotherms of DBD1 and DBD3, with the same DNA oligonucleotide containing the PRDI site, obtained by anisotropy titration at fixed temperatures in solution at pH 7.4 and 100 mM NaCl are shown in panels a and b of Figure 5. At 20 °C, the association constant is 1.1 × 10^6 M^{-1} for DBD1 and 3.6 × 10^6 M^{-1} for DBD3. The Gibbs energies obtained from these experiments are plotted against temperature in Figure 5c. They differ considerably for DBD1 and DBD3, and this difference increases with a decrease in temperature. At 20 °C and 100 mM NaCl, the Gibbs energy

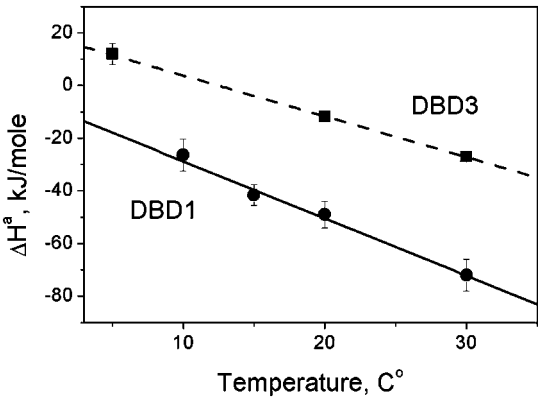

FIGURE 6: Enthalpies of association of DBD1 (—) and DBD3 (— — —) with target DNA measured by ITC at different temperatures at pH 7.4 and 100 mM NaCl.

values are -33.6 ± 1.5 and -36.7 ± 1.5 kJ/mol for DBD1 and DBD3, respectively.

An increasing salt concentration significantly affects binding of these two DBDs. In both cases, $\log(K^a)$ appears to be a linear function of log[NaCl], but the slopes of these functions $[\partial \log(K^a)/\partial \log[\mathrm{NaCl}]]$ are different: 1.4 for DBD1 and 3.3 for DBD3 (Figure 5d). Therefore, at 200 mM NaCl, these two functions cross each other, which means that under this condition the Gibbs energies of binding of these two DBDs are equal. Linear extrapolation of these functions to $\log[\mathrm{NaCl}] = 0$, i.e., to 1 M NaCl, results in very different values of association constants for these two DBDs: for DBD1 $\log(K^a)_o = 4.75$ and for DBD3 $\log(K^a)_o = 3.30$. Correspondingly, the association Gibbs energies at 1 M NaCl (ΔG^a_o) are -26.8 ± 2.0 and -18.5 ± 2.0 kJ/mol for DBD1 and DBD3, respectively

To investigate the specificities of the DBDs for their consensus PRDI site, we studied their association with DNA containing nonconsensus sequence (see Materials and Methods). At 20 °C and 100 mM NaCl, the association constant of both DBDs with this noncognate DNA dropped more than 1 order of magnitude, and for DBD1, binding did not appear to conform to a 1:1 stoichiometry (data not shown). Therefore, accurate determination of the salt effect on binding and evaluation of the components of binding energy for noncognate binding were impossible.

Enthalpy of Binding. The enthalpies of association of DBD1 and DBD3 with the target DNA measured by ITC at several fixed temperatures are presented in Figure 6. They differ significantly in magnitude; at 20 °C, ΔH^a is 40 kJ/mol greater for DBD3 than for DBD1. For DBD3, the association enthalpy is positive only at 5 °C, but for DBD1, it is negative over the entire temperature range that has been considered. With an increase in temperature, both enthalpies become more negative. Therefore, the heat capacity effect of association is negative, which indicates that apolar groups are predominantly dehydrated upon DNA binding. It is notable that ΔH^a is more temperature-dependent for DBD1 than for DBD3. The dependence of the association enthalpies on salt concentration was not studied because the association constants are low, even at 100 mM NaCl, and decrease quickly with an increase in salt concentration. Therefore, measurements of the enthalpy of association at higher salt concentrations by ITC required high concentrations of proteins, which was impossible because of the strong tendency of these proteins to aggregate. However, from the studies of other DNA binding proteins, and particularly HMG proteins, it is known that the enthalpies of association of proteins with DNA do not depend noticeably on the ionic strength of the solution (*9*, *20*, *21*).

DISCUSSION

One of the main results from this study is that free DBD1 and DBD3 differ in their stabilities; DBD3 has a more rigid structure, while DBD1 appears to be more flexible. This difference is not entirely surprising because of their low level of sequence identity (34%).

Another important result is that under standard conditions (20 °C, 100 mM NaCl, 20 mM sodium phosphate, and pH 7.4) the association constant of DBD3 for PRDI DNA is greater than that of DBD1; i.e., the Gibbs energy of association with this target DNA is significantly more negative for DBD3 than for DBD1 (Table 1). It is interesting, however, that while binding of DBD1 is enthalpy-driven, binding of DBD3 is entropy-driven. To understand the qualitative difference in the mechanisms of binding of these two DBDs, we need to analyze in detail the components of the Gibbs energy of binding.

A linear dependence between the log of the binding constant of a protein with DNA and the log of the NaCl concentration, as seen in Figure 5d, is usually regarded as a manifestation of the electrostatic interactions of this process (*20*, *22*). Formation of ion pairs between the cationic amino acids of the protein and the DNA polyanion results in the release of counterions, the mixing of which with the ions in the bulk solution produces a significant entropy increase (*22*). At relatively low concentrations of salt in the aqueous solution, when the activity of water is less affected by the presence of salt, the entropy of water release upon protein binding is independent of the salt concentration and this entropy effect is simply proportional to the number of released counterions (*23*). The counterions are released mostly from the DNA since the low charge density on protein surfaces does not attract a tight coat of counterions (*24*). Correspondingly, the logarithm of the association constant of protein with DNA is presented in just two terms:

$$\log(K^a) = \log(K^a_o) - Z\psi \log[\mathrm{NaCl}] \qquad (2)$$

where $Z\psi$ is the number of counterions released by the Z DNA phosphates upon association with protein and, correspondingly, ψ is the number of released counterions per phosphate. When the salt concentration approaches 1 M, log[NaCl] equals zero, and the electrostatic term in eq 2 becomes zero. ΔG^a_o then approximates the nonelectrostatic part of the Gibbs energy of complex formation, ΔG^a_{nel}. By subtracting this term from the overall Gibbs energy, one can calculate the electrostatic term of the Gibbs energy of binding, ΔG^a_{el} (Table 1). For the nonelectrostatic component of the Gibbs energy of association, we have then $\Delta G^a_{nel} = \Delta G^a - \Delta G^a_{el}$. Since the enthalpy of binding of protein to DNA usually does not depend on the salt concentration (*9*, *21*, *25*), it should be assigned to the nonelectrostatic component of the Gibbs energy. Then the nonelectrostatic entropy factor can be determined via the relationship $T\Delta S^a_{nel} = \Delta H^a - \Delta G^a_{nel}$, and since the electrostatic component of the Gibbs energy of association is entirely entropic in nature (*22*), we have

Table 1: Binding Characteristics of DBD1 and DBD3 to PRDI DNA at 20 °C, pH 7.4, and 100 mM NaCl[a]

	total characteristics				nonelectrostatic components			electrostatic components		
protein	ΔG^a	ΔH^a	$T\Delta S^a$	ΔC_p	ΔG^a_{nel}	ΔH^a_{nel}	$T\Delta S^a_{nel}$	ΔG^a_{el}	ΔH^a_{el}	$T\Delta S^a_{el}$
DBD1	−33.8	−50.7	−16.9	−2.2	−26.3	−50.7	−24.4	−7.5	0	7.5
DBD3	−36.7	−11.5	25.2	−1.6	−18.5	−11.5	7.0	−18.2	0	18.2
error	±1.5	±0.5	±20	±0.1	±2.0	±0.5	±2.5	±2.0		±2.0

[a] ΔG^a and ΔH^a in kilojoules per mole; ΔC_p in kilojoules per kelvin per mole.

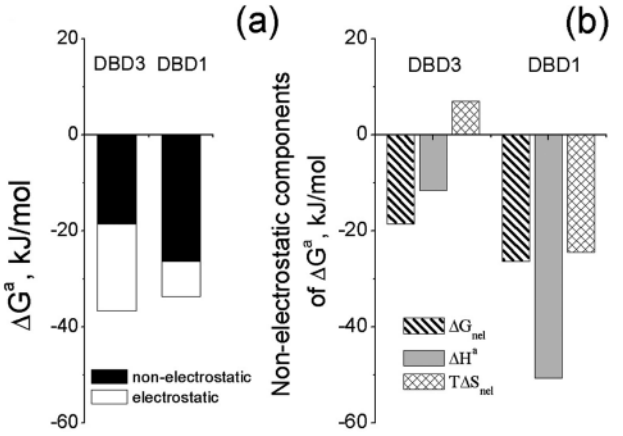

FIGURE 7: (a) Electrostatic and nonelectrostatic components of the Gibbs energy of association of DBD1 and DBD3 with target DNA duplex at 20 °C, pH 7.4, and 100 mM NaCl. (b) Enthalpic and entropic components of the nonelectrostatic Gibbs energy of association of DBD1 and DBD3 with target DNA.

for the electrostatic component of the entropy factor $TS^a_{el} = -\Delta G^a_{el}$. All these parameters of association of both DBDs with DNA at 20 °C are presented in Table 1.

It appears that the absolute value of the Gibbs energy of association of DBD3 is larger than that of DBD1 only because of its electrostatic component, while its nonelectrostatic component is smaller than that of DBD1 (Figure 7a). This is intriguing because it is known that the sequence specificity of protein−DNA interaction is determined by the nonelectrostatic component of the binding energy (*9*, *19*, *26*−*31*). Thus, association of DBD1 with DNA should be more sequence-specific than that of DBD3. It is remarkable that the larger nonelectrostatic component of the Gibbs energy of binding of DBD1 correlates with the lower stability and greater flexibility of the protein's structure. A similar correlation was observed previously with the family of HMG DNA binding proteins; the less stable, more flexible DNA binding domains of these proteins were characterized by a larger nonelectrostatic component of Gibbs energy and a higher level of DNA sequence specificity (*19*). It appears that flexible structure enables the DBD to better adjust to the structure of the DNA. That is, the protein is more complementary to the DNA, permitting it to form more base-specific contacts (*32*).

Along this line of thought, particular attention should be paid to the enthalpic and entropic components of the nonelectrostatic Gibbs energy of association of DBD1 and DBD3 with DNA (Figure 7b). It appears that the larger nonelectrostatic Gibbs energy of association of DBD1 is provided by its more negative enthalpy of binding. The nonelectrostatic entropy of binding in that case is negative; i.e., it opposes binding in contrast to the entropy of binding of DBD3, which is positive.

The positive nonelectrostatic entropy of DBD3 binding can be explained only by dehydration of the groups at the protein−DNA interface. A similar dehydration can be expected upon association of DBD1 with DNA, but its overall nonelectrostatic entropy of binding appears to be negative. Therefore, in the binding of DBD1 to DNA, the

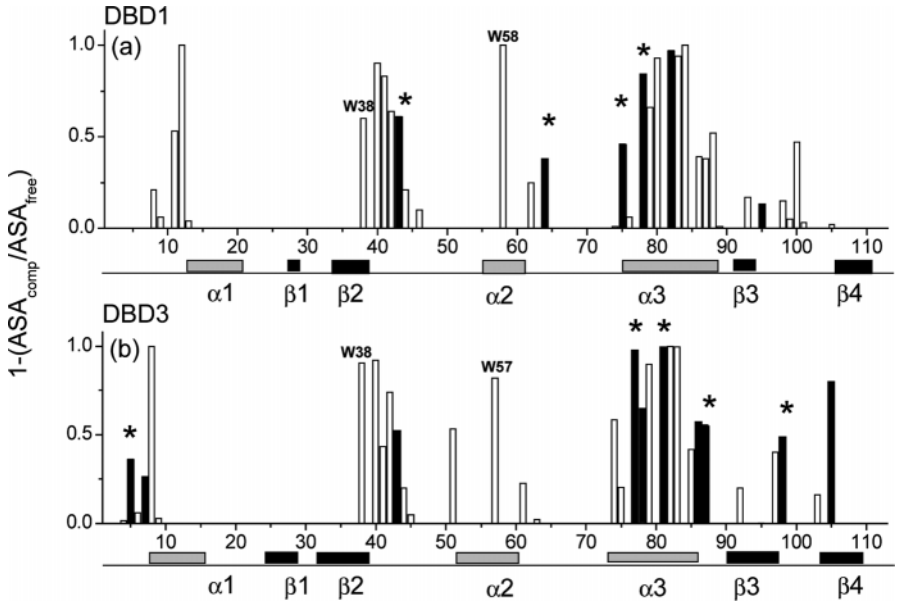

FIGURE 8: Contact map of the residues of DBD1 and DBD3 with PRDI and PRDIII DNAs. The contacts are specified by the ratio of the water accessible surface areas (ASA) of the residue in the complex with DNA and with the DNA removed from the crystal structure. In black are shown basic residues. The asterisks indicate residues that contact DNA phosphates according to the crystal structures (*2*, *4*).

positive entropy of dehydration is overbalanced by the negative entropy that might arise only from some increase in order. This cannot be the entropy associated with the loss of translational/rotational freedom because it is too small, only approximately -20 J K^{-1} mol^{-1} (*33*), and its contribution is similar in the two considered complexes. The significant negative entropy might result either from fixing some mobile substructures of DBD1 or from water incorporation in the formed interface. Some water molecules were indeed found to be incorporated into the crystal structures of DBD1 and DBD2 complexes with DNA (*2*, *7*). It is unclear, however, why more water molecules would be incorporated in the DBD1−DNA complex than in the DBD3−DNA complex. On the other hand, the crystal structures show that loops L1 and L3 of both DBDs participate directly in DNA binding, and the loops of DBD1 are more extended (Figure 1). The structure of DBD2 shows that loops L1 and L3 are disordered in solution but undergo large conformational changes upon binding DNA (*6*, *7*). From the thermodynamic studies presented above, we know that free DBD1 has a much looser structure, and its entropy of unfolding is significantly lower than that of DBD3. This large disparity provides evidence that the difference in the nonelectrostatic entropies of association of the DBDs results mainly from the difference in the extension and flexibility of the loops participating directly in DNA binding, which should certainly be fixed by their interactions with DNA.

Another question that arises is why the electrostatic component in binding energy prevails in the DBD3−DNA complex (Figure 7a). In other words, why is the dependence of $\log(K^a)$ on log[NaCl] significantly stronger for DBD3 binding to DNA (Figure 5d)? According to eq 2, the slope of this function determines the number of counterions released by the DNA phosphates upon protein binding, which appears to be 1.4 and 3.3 for DBD1 and DBD3, respectively. If $\psi = 0.64$, as suggested for short DNA duplexes (*21*), we find that *Z*, the number of phosphates releasing counterions, is ~2.2 for DBD1 association and ~5 for DBD3 association. Thus, DBD1 forms approximately 2 times fewer charge−charge contacts with DNA phosphates than DBD3. Analysis of the crystal structures of DBD1−PRDI and DBD3−PRDIII complexes presented in the contact maps in Figure 8 shows also that these two complexes differ in the number of ionic contacts: DBD1 has 6 positive charges contacting PRDI DNA, while DBD3 has 10 positive charges contacting PRDIII DNA. It appears, however, that not all of these contacts are with phosphates; i.e., not all of the DNA-contacting residues are responsible for the release of counterions upon complex formation: the number of contacts of basic residues (Arg and Lys) of the protein with DNA phosphates is 4 for DBD1 and 5 for DBD3. These residues are denoted with asterisks in Figure 8. The correspondence of these values with the results of titration experiment is perfect for the DBD3 complex, although the DNAs used in these two experiments were not identical. In the case of the DBD1−PRDI complex, the correspondence of the crystal and titration data is less impressive, although the DNA used in these two experiments was identical. It is certain, however, that DBD3 makes significantly more ionic contacts with DNA phosphates than DBD1.

ACKNOWLEDGMENT

We thank Dr. Carlos Escalante for providing the plasmids encoding IRF-1 DBD and IRF-3 DBD.

REFERENCES

1. Nguyen, H., Hiscott, J., and Pitha, P. M. (1997) The growing family of interferon regulatory factors, *Cytokine Growth Factor Rev. 8*, 293−312.
2. Escalante, C. R., Yie, J., Thanos, D., and Aggarwal, A. K. (1998) Structure of IRF-1 with bound DNA reveals determinants of interferon regulation, *Nature 391*, 103−6.
3. Kusumoto, M., Fujii, Y., Tsukuda, Y., Ohira, T., Kyougoku, Y., Taniguchi, T., and Hakoshima, T. (1998) Crystallographic characterization of the DNA-Binding Domain of Interferon Regulatory Factor-2 complexed with DNA, *J. Struct. Biol. 121*, 363−6.
4. Panne, D., Maniatis, T., and Harrison, S. C. (2004) Crystal structure of ATF-2/c-Jun and IRF-3 bound to the interferon-β enhancer, *EMBO J. 23*, 4384−93.
5. Escalante, C. R., Brass, A. L., Pongubala, J. M., Shatova, E., Shen, L., Singh, H., and Aggarwal, A. K. (2002) Crystal structure of PU.1/IRF-4/DNA ternary complex, *Mol. Cell 10*, 1097−105.
6. Furui, J., Uegaki, K., Yamazi, T., Shirakawa, M., Swindells, M. B., Harada, H., Taniguchi, T., and Kyogoku, Y. (1998) Solution structure of the IRF-2 DNA-binding domain: A novel subgroup of the winged helix-turn-helix family, *Structure 6*, 491−500.
7. Fujii, Y., Shimizu, T., Kusumoto, M., Kyogoku, Y., Taniguchi, T., and Hakoshima, T. (1999) Crystal structure of an IRF-DNA complex reveals novel DNA recognition and cooperative binding to a tandem repeat of core sequences, *EMBO J. 18*, 5028−41.
8. Escalante, C. R., Yie, J., Thanos, D., and Aggarwal, A. K. (1997) Expression, purification, and co-crystallization of IRF-I bound to the interferon-β element PRD I, *FEBS Lett. 414*, 219−20.
9. Dragan, A. I., Klass, J., Read, C., Churchill, M. E., Crane-Robinson, C., and Privalov, P. L. (2003) DNA binding of a non-sequence-specific HMG-D protein is entropy driven with a substantial non-electrostatic contribution, *J. Mol. Biol. 331*, 795−813.
10. Privalov, G., Kavina, V., Freire, E., and Privalov, P. L. (1995) Precise scanning calorimeter for studying thermal properties of biological macromolecules in dilute solution, *Anal. Biochem. 232*, 79−85.
11. Privalov, P. L., and Potekhin, S. A. (1986) Scanning microcalorimetry in studying temperature-induced changes in proteins, *Methods Enzymol. 131*, 4−51.
12. Privalov, G. P., and Privalov, P. L. (2000) Problems and prospects in microcalorimetry of biological macromolecules, *Methods Enzymol. 323*, 31−62.
13. Privalov, P. L., and Makhatadze, G. I. (1990) Heat capacity of proteins. II. Partial molar heat capacity of the unfolded polypeptide chain of proteins: Protein unfolding effects, *J. Mol. Biol. 213*, 385−91.
14. Hackel, M., Hinz, H. J., and Hedwig, G. R. (1999) A new set of peptide-based group heat capacities for use in protein stability calculations, *J. Mol. Biol. 291*, 197−213.
15. Pace, C. N., Laurents, D. V., and Thomson, J. A. (1990) pH dependence of the urea and guanidine hydrochloride denaturation of ribonuclease A and ribonuclease T1, *Biochemistry 29*, 2564−72.
16. Spolar, R. S., Livingston, J. R., and Record, M. T., Jr. (1992) Use of liquid hydrocarbon and amide transfer data to estimate contributions to thermodynamic functions of protein folding from the removal of non-polar and polar surfaces from water, *Biochemistry 31*, 3947−55.
17. Privalov, P. L., and Makhatadze, G. I. (1992) Contribution of hydration and non-covalent interactions to the heat capacity effect on protein unfolding, *J. Mol. Biol. 224*, 715−23.
18. Spolar, R. S., and Record, M. T., Jr. (1994) Coupling of local folding to site-specific binding of proteins to DNA, *Science 263*, 777−84.
19. Dragan, A. I., Read, C. M., Makeyeva, E. N., Milgotina, E. I., Churchill, M. E. A., Crane-Robinson, C., and Privalov, P. L. (2004) DNA binding and bending by HMG boxes: Energetic determinants of specificity, *J. Mol. Biol. 343*, 371−93.
20. Record, M. T., Jr., Anderson, C. F., and Lohman, T. M. (1978) Thermodynamic analysis of ion effects on the binding and conformational equilibria of proteins and nucleic acids: The roles

of ion association or release, screening, and ion effects on water activity, *Q. Rev. Biophys. 11*, 103−78.
21. Olmstead, M. C., Bond, J. P., Anderson, C. F., and Record, M. T., Jr. (1995) Grand canonical Monte Carlo molecular and thermodynamic predictions of ion effects on binding of an oligocation (L8+) to the center of DNA oligomers, *Biophys. J. 68*, 634−47.
22. Manning, G. S. (1978) The molecular theory of polyelectrolyte solutions with applications to the electrostatic properties of polynucleotides, *Q. Rev. Biophys. 11*, 179−246.
23. Ha, J. H., Capp, M. W., Hohenwalter, M. D., Baskerville, M., and Record, M. T., Jr. (1992) Thermodynamic stoichiometries of participation of water, cations and anions in specific and non-specific binding of lac repressor to DNA. Possible thermodynamic origins of the "glutamate effect" on protein-DNA interactions, *J. Mol. Biol. 228*, 252−64.
24. Manning, G. S. (2003) Is a small number of charge neutralizations sufficient to bend nucleosome core DNA onto its superhelical ramp? *J. Am. Chem. Soc. 125*, 15087−92.
25. Record, M. T., Jr., Zhang, W., and Anderson, C. F. (1998) Analysis of effects of salts and uncharged solutes on protein and nucleic acid equilibria and processes: A practical guide to recognizing and interpreting polyelectrolyte effects, Hofmeister effects, and osmotic effects of salts, *Adv. Protein Chem. 51*, 281−353.
26. Revzin, A., and von Hippel, P. H. (1977) Direct measurement of association constants for the binding of *Escherichia coli* lac repressor to non-operator DNA, *Biochemistry 16*, 4769−76.
27. DeHaseth, P. L., Lohman, T. M., and Record, M. T., Jr. (1977) Nonspecific interaction of lac repressor with DNA: An association reaction driven by counterion release, *Biochemistry 16*, 4783−90.
28. Boschelli, F. (1982) Lambda phage cro repressor. Non-specific DNA binding, *J. Mol. Biol. 162*, 267−82.
29. Matthew, J. B., and Ohlendorf, D. H. (1985) Electrostatic deformation of DNA by a DNA-binding protein, *J. Biol. Chem. 25*, 5860−2.
30. Takeda, Y., Ross, P. D., and Mudd, C. P. (1992) Thermodynamics of Cro-DNA interactions, *Proc. Natl. Acad. Sci. U.S.A. 89*, 8180−4.
31. Ha, J. H., Spolar, R. S., and Record, M. T., Jr. (1989) Role of the hydrophobic effect in stability of site-specific protein-DNA complexes, *J. Mol. Biol. 209*, 801−16.
32. Wright, P. E., and Dyson, H. J. (1999) Intrinsically unstructured proteins: Re-assessing the protein structure−function paradigm, *J. Mol. Biol. 293*, 321−31.
33. Tamura, A., and Privalov, P. L. (1997) The entropy cost of protein association, *J. Mol. Biol. 273*, 1048−60.

BI051115O